CrystEngComm

COMMUNICATION

View Article Online
View Journal | View Issue

Cite this: *CrystEngComm*, 2015, **17**, 1902

Received 5th December 2014,
Accepted 21st January 2015

DOI: 10.1039/c4ce02405b

www.rsc.org/crystengcomm

Homogenously hexagonal prismatic $AgBiS_2$ nanocrystals: controlled synthesis and application in quantum dot-sensitized solar cells†

Na Liang,[a] Wenlong Chen,[a] Fang Dai,[b] Xiangyang Wu,[c] Wei Zhang,[c] Zhi Li,[c] Jingmei Shen,[b] Shoushuang Huang,[a] Qingquan He,[a] JiantaoZai,*[a] Nenghu Fang[a] and Xuefeng Qian*[a]

Homogenously hexagonal prismatic $AgBiS_2$ nanocrystals with sizes of about 7.6 nm have been synthesized by the selective absorption of oleylamine and anisotropic growth in a mixed solvent system. Quantum dot-sensitized solar cells with the as-prepared $AgBiS_2$ nanocrystals as counterelectrode materials showed a conversion efficiency of 2.09% compared with that of Pt (1.73%).

Quantum dot-sensitized solar cells (QDSSCs) have attracted much attention as third-generation photovoltaic cells due to their promising energy conversion efficiency, low cost and simple cell structure.[1] QDSSCs borrow the similar working principle of dye sensitized solar cells (DSSCs) with the replacement of dye by semiconductor quantum dots (QDs).[2] In past years, much effort had focused on the modification of photoelectrodes, including the optimization of TiO_2 films and the formation of a new variety of QD sensitizers to improve the performance of QDSSCs.[3] Apart from the design of photoelectrodes, reasonable selection of a counterelectrode (CE) as well as an electrolyte is also considerably important to improve the performance of QDSSCs. However, few multiternary chalcogenides have been applied to QDSSCs as CE materials because of their difficult synthesis methods.

As a typical member of I–V–VI_2 ternary chalcogenides, $AgBiS_2$ exhibits flexible properties and has been widely applied in thermoelectric devices[4] and photoelectrode sensitizers.[5] Various approaches, such as hot-injection, solvothermal and microwave refluxing methods, have been developed to produce $AgBiS_2$ with different morphologies, *e.g.* nanoparticles and nanostructured flowers.[8,10,11] For instance, Chen *et al.* prepared $AgBiS_2$ nanoparticles with an irregular shape by a hot-injection method.[6] However, homogenous $AgBiS_2$ nanoparticles with a regular morphology are rarely prepared. Herein, homogenous $AgBiS_2$ nanocrystals with a hexagonal prismatic shape were firstly prepared by the selective absorption of oleylamine (OA) and anisotropic growth in a mixed solvent system, and a plausible formation mechanism of the $AgBiS_2$ nanocrystals was proposed. Furthermore, the as-prepared $AgBiS_2$ nanocrystals were used as CE materials for QDSSCs, verifying their commendable electrocatalytic activity toward polysulfide reduction compared with Pt.

$AgBiS_2$ nanocrystals were synthesized in a mixed solvent by a solvothermal process. In a typical process, 0.3 mmol of AgAc and 1.2 g of OA were dissolved in 25 mL of mixed solvent of cyclohexane (CHA) and 1-decyl alcohol (DCA) (V : V = 1 : 1) at room temperature. Then 0.3 mmol of $BiCl_3$ and 0.5 mL of CS_2 were added. After being reacted in an autoclave at 200 °C for 12 hours and cooled to 60 °C naturally, a precipitate was obtained after 5 mL of methanol was added and washed with absolute ethanol. Finally, the product was dried at 60 °C for 4 hours in a vacuum oven. Experimental details, including the preparation of photoelectrodes, counterelectrodes and solar cells, are described in the ESI.†

The morphology of the as-prepared $AgBiS_2$ nanocrystals was studied by transmission electron microscopy (TEM), high resolution TEM (HRTEM) and their simulated structure insert. Fig. 1a shows that the obtained products are of 1-D chain superstructure, built by uniform nanocrystals. Magnified images (Fig. 1b and c) reveal that the built units, in fact, are of hexagonal prismatic nanocrystals (Fig. 1a), in which the square morphology is due to the side of $AgBiS_2$ nanocrystals lying on the copper mesh (Fig. 1b), while the hexagonal morphology is due to the $AgBiS_2$ nanocrystals directly standing on the copper mesh (Fig. 1c). The obtained nanocrystals are homogenous with narrow size distribution (Fig. S1†), and the average size is about 7.6 nm. Furthermore, the distance between chains is around 2.26 nm (Fig. S2†). This value is less than the length of OA, which is calculated to be 2.54 nm. The theoretical

[a] *Shanghai Electrochemical Energy Devices Research Center, School of Chemistry and Chemical Engineering and State Key Laboratory of Metal Matrix Composites, Shanghai Jiao Tong University, Shanghai, 200240, PR China.*
E-mail: xfqian@sjtu.edu.cn, zaijiantao@sjtu.edu.cn
[b] *Global Research & Development, General Motors, MI 48090, USA*
[c] *Shanghai Key Laboratory of Catalysis of Polyolefin, Shanghai Research Institute of Chemical Industry, Shanghai 200062, PR China*

† Electronic supplementary information (ESI) available. See DOI: 10.1039/c4ce02405b

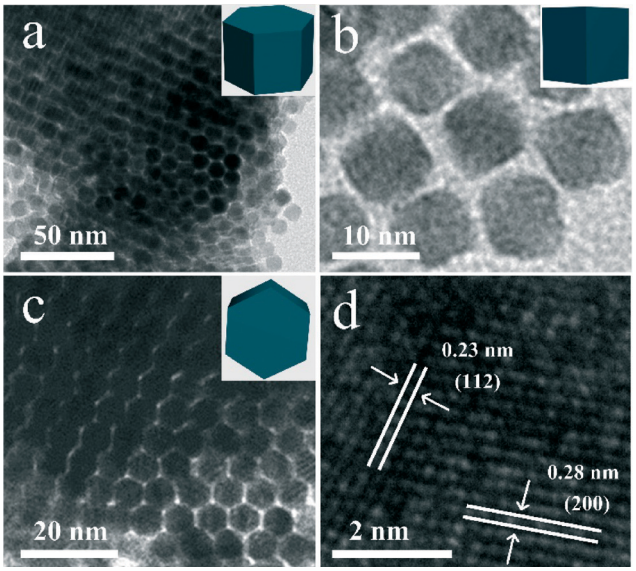

Fig. 1 (a) TEM and (b–d) HRTEM images of the as-prepared $AgBiS_2$ nanocrystals and the insets are the simulated structures.

value can be predicted by the formula L (nm) = 0.25 + 0.127n, where n is the number of carbon atoms in the alkyl chain.[7] The above results indicate that the obtained nanocrystals are homogenous and enwrapped by a layer of OA, which interpenetrate neighbouring OA on a $AgBiS_2$ nanocrystal surface.[8] In the HRTEM image of the $AgBiS_2$ nanocrystal (Fig. 1d), the lattice spacings of 0.23 and 0.28 nm are also close to the (112) and (200) lattice planes of cubic $AgBiS_2$, indicating their high crystallinity.

Fig. 2a shows the XRD pattern of the obtained $AgBiS_2$ nanocrystals. It can be seen that all diffraction peaks can be indexed well as the cubic $AgBiS_2$ (JCPDS card no. 21-1178). The lattice spacing calculated based on the (200) peak is 0.28 nm, which is consistent with the HRTEM image and the crystal structure. No other impurities, such as Ag_2S[9] and Bi_2S_3,[10] are detected. X-ray photoelectron spectroscopy (XPS) was used to characterize the composition and surface electron state of the $AgBiS_2$ nanocrystals. The signals of Ag, Bi and S in the full spectrum suggest that the as-prepared sample is $AgBiS_2$ (Fig. 2b). The high resolution XPS spectra of Ag3d, Bi4f and S2s are shown in Fig. S3.† The peaks of $Ag3d_{3/2}$ and $Ag3d_{5/2}$ at 373.6 and 367.7 eV are consistent with the standard Ag. Apart from the main peaks, no other satellite

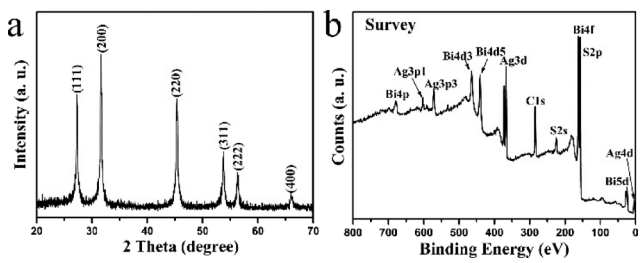

Fig. 2 (a) XRD pattern and (b) XPS spectrum of the as-prepared $AgBiS_2$ nanocrystals.

peaks on the high binding energy side of the Ag3d peak imply that no by-products, such as Ag_2S[11] and Ag_2O, were formed.[12] The peaks at 163.7 and 158.1 eV correspond to $Bi4f_{5/2}$ and $Bi4f_{7/2}$, and the peak at 161.31 eV can be attributed to Bi5s binding energy, matching well with Bi.[13,14] The binding energy of S2s is located at 225.4 eV.[4] Similar results are also observed in the previous studies on $AgBiS_2$.[13,14]

In general, the growth of nanocrystals is usually followed by the crystal habit and reaction conditions, and the shape of a face-centered cubic (fcc) nanocrystal is mainly determined by the growth rates along the <200> direction and the <222> direction.[15] The driving force for the transformation from a cube to a polyhedron lies in the fact that the growth rate along the <200> direction is higher than that along the <222> direction, since the free energy of {200} facets is obviously higher than that of the {222} facets. Thus $AgBiS_2$ seeds would prefer to grow along the <200> direction, and lead to the eventual disappearance of {200} facets in the final products.[16] However, the {200} facets are still maintained in the obtained $AgBiS_2$ because of the effect of OA with a long carbon chain in this system. On the other hand, from the viewpoint of the crystal structure of $AgBiS_2$ (Fig. S4†), as the {200} facets consist of Ag^+, Bi^{3+} and S^{2-}, OA would preferentially absorb onto the {200} facets due to the combination interaction between metal cations and OA.[17] So the growth of {200} facets would be reduced because these facets are passivated by OA, and the {112} facets appear.[15] Ultimately, hexagonal prismatic $AgBiS_2$ nanocrystals form as the reaction continues.

Due to the large different values of K_{sp} between Ag_2S ($10^{-49.2}$) and Bi_2S_3 (10^{-97}), separated binary compounds are often obtained. Thus, suitable reaction conditions are important to form $AgBiS_2$ and tune its morphology. In this work, a mixed solvent (CHA and DCA) is designed to tune the reaction activity of metal precursors and the morphology of the final products (Fig. S5†). When the volume ratio of CHA to DCA is 1 : 6, irregular $AgBiS_2$ nanocrystals with larger blocks

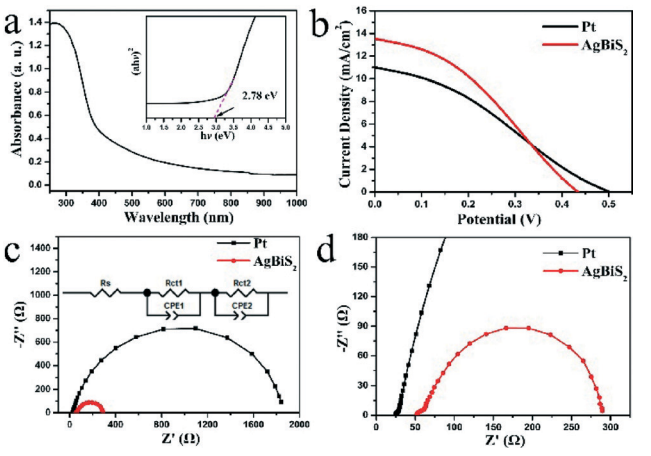

Fig. 3 (a) UV-vis absorption spectrum of $AgBiS_2$ nanocrystals. (b) J–V curves of QDSSCs with Pt and $AgBiS_2$ as counterelectrodes. (c) EIS spectra of Pt and $AgBiS_2$ electrodes (inset of (c) is an equivalent circuit employed to fit the EIS spectra). (d) Magnified plots of (c).

Table 1 Photovoltaic and EIS parameters of the Pt and $AgBiS_2$ based CEs

CE sample	J_{sc}, mA cm^{-2}	V_{oc}, V	FF	η, %	R_S, Ω cm^2	R_{ct1}, Ω cm^2	CPE_1, μF	R_{ct2}, Ω cm^2	CPE_2, μF
Pt	11.0	0.50	0.31	1.73	26.1	2.94	4.70	895	41.7
$AgBiS_2$	13.5	0.43	0.36	2.09	26.2	3.20	76.5	49.2	184

are obtained (Fig. S5a†). With the volume ratio of CHA to DCA increasing to 1 : 3, blocks disappear gradually (Fig. S5b†), and homogenously hexagonal prismatic $AgBiS_2$ nanocrystals with sizes of about 7.6 nm are obtained when the volume ratio of CHA to DCA is up to 1 : 1 (Fig. S5c†). However, further increasing the volume ratio of CHA : DCA to 3 : 1 or 6 : 1, $AgBiS_2$ nanocrystals grow larger, and they tend to aggregate (Fig. S5d and e†). The above results suggest that the mixed solvents affect the nucleation and morphology of $AgBiS_2$ nanocrystals.

Further studies reveal that the reaction time and the amount of OA also have important effects on the phase and morphology of $AgBiS_2$ nanocrystals (Fig. S6†). Irregular $AgBiS_2$ nanocrystals are obtained within 3 hours (Fig. S6a†), and homogenous nanocrystals that tend to assemble into superstructures are obtained when the reaction time is prolonged to 6 or 12 hours (Fig. S6b and c†). However, if the reaction time is up to 16 or 24 hours, $AgBiS_2$ superstructures disappear and the size of $AgBiS_2$ nanocrystals increases because of the famous Ostwald ripening process (Fig. S6d–e†).[18] On the other hand, the amount of OA also affects the phase and morphology of the final products. It is generally accepted that OA containing both solvophilic and metal coordinating groups is often used as a capping reagent to prepare nanomaterials. OA could solvate nanocrystals and further control the size or morphology of the obtained products.[19,20] Fig. S7† shows the TEM images of the as-prepared products with different amounts of OA. By-product Bi_2S_3 is detected besides $AgBiS_2$ when 0.3 g of OA is used (Fig. S7a and f†). When the amount of OA is in the range of 0.6 and 1.2 g, hexagonal prismatic $AgBiS_2$ nanocrystals are obtained, and they tend to self-assemble into superstructures. However, too little (Fig. S7a and b†) or too much (Fig. S7e†) OA would lead to irregular particles because of less control or over-passivation of OA on $AgBiS_2$ nanocrystals. Fig. 3a shows the UV-vis absorption spectrum of the as-prepared $AgBiS_2$ nanocrystals, and they have optical absorption in the visible region. $AgBiS_2$ is the direct transition (n = 1/2),[5] and its band gap energy (E_g) is 2.78 eV, determined from the absorbance spectra according to the equation (ESI†).

The as-prepared $AgBiS_2$ nanocrystals were fabricated as CE in QDSSCs to investigate their photovoltaic performance. The CEs based on Pt were also fabricated for comparison. The current density–voltage (J–V) curves of the QDSSCs with $AgBiS_2$ nanocrystals and Pt CEs are shown in Fig. 3b, and their photovoltaic parameters are summarized in Table 1. It can be seen that the QDSSC fabricated with the $AgBiS_2$ nanocrystal CE exhibits a short circuit current (J_{sc}) of 13.54 mA cm^{-2}, an open-circuit voltage (V_{oc}) of 0.43 V and a fill factor (FF) of 0.36, yielding an overall power conversion efficiency (η) of 2.09%, which is comparable to the reference Pt devices with a J_{sc} of 11.01 mA cm^{-2}, a FF of 0.31, and an η value of 1.73%. The inferior performance of QDSSCs to Pt CE may be due to the low catalytic activity of Pt in polysulfide electrolytes. Electrochemical impedance spectroscopy (EIS) was employed to investigate the charge transfer resistances.[3,21] The Nyquist plots are presented in Fig. 3c and d, and the resulting parameters are summarized in Table 1. One can see that the first high-frequency arches are related to the solid–solid interface resistance (R_{ct1}), the second semicircles in the lower frequency range is associated with the electron transfer at the solid/electrolyte interface (R_{ct2}) (inset in Fig. 3c). In the Nyquist plots, the high-frequency intercepts arise from sheet resistances (R_S), transfer resistance (R_{ct2}) at the CE/electrolyte interface and double layer capacitance (CPE).[22] The R_S values of Pt and $AgBiS_2$ CE are similar, and the R_{ct1} value in each CE film is not significantly different (R_{ct1} of Pt is smaller than that of $AgBiS_2$ because of the better conductivity of Pt). Notably, the radius of the second semi-circle of the Pt CE is bigger than that of $AgBiS_2$ CE (Fig. 3d) as shown in the detailed EIS data, and $AgBiS_2$ CE possesses a smaller value of R_{ct2} (49.16 Ω cm^2) than Pt CE (895.2 Ω cm^2), reflecting that the charge transfer from $AgBiS_2$ CE to polysulfides is easier than that from Pt CEs.[23] It is well known that CPE values can reflect the roughness and surface area of electrodes.[22,24] Comparing the reference Pt CE, the high CPE_1 and CPE_2 suggest that $AgBiS_2$ CE has a larger surface area and can supply more electrocatalytic sites. The facilitated charge transfer (R_{ct2}) from CE to polysulfide electrolyte and more electrocatalytic active sites would result in $AgBiS_2$ CE with higher electrocatalytic activity towards the reduction of polysulfides and better performance of QDSSCs compared with those of Pt CE.

In conclusion, homogenously hexagonal prismatic $AgBiS_2$ nanocrystals with sizes of around 7.6 nm have been synthesized in a mixed solvent system by a facile solvothermal process. The obtained nanocrystals tended to self-assemble into ordered superstructures because of their suitable morphology and size and the modification of OA. A plausible mechanism for the formation of the special structures was also proposed. The as-prepared $AgBiS_2$ nanocrystals were fabricated as CEs for QDSSCs, and they exhibited a higher conversion efficiency of 2.09%, which is higher than that of the reference Pt CE (1.73%) under a light intensity of 100 mW cm^{-2}. The work suggests that the ternary chalcogenides are potential candidates as low-cost counterelectrode catalysts in QDSSCs.

Acknowledgements

The work was supported by the Shanghai Nano Project (12nm0504300), the National Natural Science Foundation of

China (21371121 and 21331004), the Open Funds of SKLMMC of SJTU (mmc-kf14-09), and the Science and Technology Commission of Shanghai Municipality (14DZ2250800).

Notes and references

1 A. J. Nozik, M. C. Beard, J. M. Luther, M. Law, R. J. Ellingson and J. C. Johnson, *Chem. Rev.*, 2010, **110**, 6873–6890.
2 B. O'Regan and M. Gratzel, *Nature*, 1991, **353**, 737–740.
3 Y. Yang, L. Zhu, H. Sun, X. Huang, Y. Luo, D. Li and Q. Meng, *ACS Appl. Mater. Interfaces*, 2012, **4**, 6162–6168.
4 S. N. Guin and K. Biswas, *Chem. Mater.*, 2013, **25**, 3225–3231.
5 P. C. Huang, W. C. Yang and M. W. Lee, *J. Phys. Chem. C*, 2013, **117**, 18308–18314.
6 C. Chen, X. Qiu, S. Ji, C. Jia and C. Ye, *CrystEngComm*, 2013, **15**, 7644–7648.
7 C. D. Bain, J. Evall and G. M. Whitesides, *J. Am. Chem. Soc.*, 1989, **111**, 7155–7164.
8 A. Badia, W. Gao, S. Singh, L. Demers, L. Cuccia and L. Reven, *Langmuir*, 1996, **12**, 1262–1269.
9 X. Wang, S. Zhan, Y. Wang, P. Wang, H. Yu, J. Yu and C. Hu, *J. Colloid Interface Sci.*, 2014, **422**, 30–37.
10 Y. Luo, H. Chen, X. Li, Z. Gong, X. Wang, X. Peng, M. He and Z. Sheng, *Mater. Lett.*, 2013, **105**, 12–15.
11 G. Hota, S. B. Idage and K. C. Khilar, *Colloids Surf., A*, 2007, **293**, 5–12.
12 X. Y. Gao, S. Y. Wang, J. Li, Y. X. Zheng, R. J. Zhang, P. Zhou, Y. M. Yang and L. Y. Chen, *Thin Solid Films*, 2004, **455–456**, 438–442.
13 J. Zhong, W. Xiang, C. Xie, X. Liang and X. Xu, *Mater. Chem. Phys.*, 2013, **138**, 773–779.
14 H. Liu, J. Zhong, X. Liang, J. Zhang and W. Xiang, *J. Alloys Compd.*, 2011, **509**, L267–L272.
15 P. Zhang, Y. Sui, G. Xiao, Y. Wang, C. Wang, B. Liu, G. Zou and B. Zou, *J. Mater. Chem. A*, 2013, **1**, 1632–1638.
16 M. Jin, H. Zhang, Z. Xie and Y. Xia, *Energy Environ. Sci.*, 2012, **5**, 6352–6357.
17 W. Du, X. Qian, J. Yin and Q. Gong, *Chem. – Eur. J.*, 2007, **13**, 8840–8846.
18 W. Du, X. Qian, X. Ma, Q. Gong, H. Cao and J. Yin, *Chem. – Eur. J.*, 2007, **13**, 3241–3247.
19 Y. Yuan, J. Zai, Y. Su and X. Qian, *J. Solid State Chem.*, 2011, **184**, 1227–1235.
20 I. J. Kramer and E. H. Sargent, *Chem. Rev.*, 2013, **114**, 863–882.
21 V. González-Pedro, X. Xu, I. Mora-Seró and J. Bisquert, *ACS Nano*, 2010, **4**, 5783–5790.
22 A. Hauch and A. Georg, *Electrochim. Acta*, 2001, **46**, 3457–3466.
23 S. C. Riha, D. C. Johnson and A. L. Prieto, *J. Am. Chem. Soc.*, 2010, **133**, 1383–1390.
24 T. N. Murakami, S. Ito, Q. Wang, M. K. Nazeeruddin, T. Bessho, I. Cesar, P. Liska, R. Humphry-Baker, P. Comte, P. Péchy and M. Grätzel, *J. Electrochem. Soc.*, 2006, **153**, A2255–A2261.